A fully coupled 3D wave-current interaction model on unstructured grids

Aron Roland,[1] Yinglong J. Zhang,[2,4] Harry V. Wang,[3] Yanqiu Meng,[3] Yi-Cheng Teng,[3] Vladimir Maderich,[5] Igor Brovchenko,[5] Mathieu Dutour-Sikiric,[6] and Ulrich Zanke[1]

Received 31 January 2012; revised 13 August 2012; accepted 21 August 2012; published 29 September 2012.

[1] We present a new modeling system for wave-current interaction based on unstructured grids and thus suitable for very large-scale high-resolution multiscale studies. The coupling between the 3D current model (SELFE) and the 3rd generation spectral wave model (WWM-II) is done at the source code level and the two models share same sub-domains in the parallel MPI implementation in order to ensure parallel efficiency and avoid interpolation. We demonstrate the accuracy, efficiency, stability and robustness of the coupled SELFE-WWM-II model with a suite of progressively challenging benchmarks with analytical solution, laboratory data, and field data. The coupled model is shown to be able to capture important physics of the wave-current interaction under very different scales and environmental conditions with excellent convergence properties even in complicated test cases. The challenges in simulating the 3D wave-induced effects are highlighted as well, where more research is warranted.

Citation: Roland, A., Y. J. Zhang, H. V. Wang, Y. Meng, Y.-C. Teng, V. Maderich, I. Brovchenko, M. Dutour-Sikiric, and U. Zanke (2012), A fully coupled 3D wave-current interaction model on unstructured grids, *J. Geophys. Res.*, *117*, C00J33, doi:10.1029/2012JC007952.

1. Introduction

[2] The interaction of ocean waves and currents is a fast evolving research topic and is shown to be of great importance for various applications, ranging from weather forecasting e.g., SST predictions [e.g., *Takaya et al.*, 2010], surface currents that are strongly influenced by Stokes' drifts due to wave motion [e.g., *Ardhuin et al.*, 2009] and applications at the coastal zone, where waves can have a strong contribution to the water levels and the littoral processes [*Bowen*, 1969; *Longuet-Higgins and Stewart*, 1963].

[3] The nonlinear interaction between long-period "currents" (e.g., tidal circulation) and short-period (<30 s) "waves" plays an especially important role in the nearshore "surf" zone, through at least the following three mechanisms: (1) the wave momentum flux that can be represented by "radiation stresses" [*Longuet-Higgins and Stewart*, 1962], or the combination of vortex force, Bernoulli head and momentum loss associated with breaking [*McWilliams et al.*, 2004; *Ardhuin et al.*, 2008]; (2) wave-induced surface roughness, stress, and surface mixing [e.g., *Janssen*, 1989, 1991, 2001; *Craig and Banner*, 1994]; (3) wave-induced bottom stress in shallow waters [*Grant and Madsen*, 1979, hereinafter GM79; *Xie et al.*, 2001). Other important mechanisms include the Stokes drift generated by the waves [*Ardhuin et al.*, 2009; *Bennis and Ardhuin*, 2011].

[4] The new advancements in the theoretical framework notwithstanding, the ultimate validation of the new wave-current interaction formulations needs to be carried out with realistic and consistent numerical models at contrasting scales from O(1 m) to O(1000 km) and beyond (e.g., global wave climate). Several fully coupled wave-current models have been proposed in the past decade [e.g., *Xia et al.*, 2004; *Xie et al.*, 2001; *Warner et al.*, 2008; *Uchiyama et al.*, 2010], most of which are based on structured-grid formulation due to its inherent simplicity. However, the complexity of the geometry and bathymetry nearshore, and the critical need for high-resolution under contrasting spatial and temporal scales provide an ideal setting for the use of unstructured-grid technique [*Dietrich et al.*, 2011]. The advantages of using unstructured-grid models as well as relative merit of each unstructured-grid model (including the present SELFE-WWMII) are being carefully investigated in a NOAA/IOOS sponsored project for U.S. east coast and Gulf of Mexico (SURA/inundation project, 2011).

[5] In this work we introduce a community-driven, parallel and innovative numerical framework that can be utilized to study the wave-current interaction processes based on unstructured meshes in geographical space. We shall only introduce the basic numerical building blocks that pave the

[1]Institute for Hydraulic and Water Resources Engineering, Technische Universität Darmstadt, Darmstadt, Germany.
[2]Center for Coastal Margin Observation and Prediction, Oregon Health and Science University, Beaverton, Oregon, USA.
[3]Virginia Institute of Marine Science, Gloucester Point, Virginia, USA.
[4]Now at Virginia Institute of Marine Science, Gloucester Point, Virginia, USA.
[5]Institute of Mathematical Machine and System Problems, National Academy of Sciences of Ukraine, Kiev, Ukraine.
[6]Institut Ruder Boskovic, Zagreb, Croatia.

Corresponding author: Y. J. Zhang, Center for Coastal Resources Management, Virginia Institute of Marine Science, 1375 Greate Rd., P.O. Box 1346, Gloucester Point, VA 23062, USA. (yjzhang@vims.edu)

0148-0227/12/2012JC007952

way for future development in this field. In particular we have coupled the wind wave model (WWM-II) [*Roland*, 2009] to the circulation model SELFE [*Zhang and Baptista*, 2008a], accounting for the wave induced momentum flux from waves to currents, based on the radiation stress formulations according to *Longuet-Higgins and Stewart* [1964], the Wave Boundary Layer (WBL) according to the theory of *Grant and Madsen* [1979], surface mixing following *Craig and Banner* [1994], and the current induced Doppler shift for waves [*Komen et al.*, 1994]. Our work constitutes one of the first attempts to couple a 3D unstructured-grid current model to a wave model, and our experience demonstrates that the stability and robustness of the two types of models are essential for ensuring consistent and convergent model results.

[6] The new model is especially suitable for the study of the combined wave-current action in very large field-scale applications. The current model is based on SELFE, originally proposed by *Zhang and Baptista* [2008a] and applied by many others [*Burla et al.*, 2010; *Bertin et al.*, 2009; *Brovchenko et al.*, 2011]. As a 3D hydrodynamic model (with unstructured triangular grid in the horizontal and hybrid terrain-following *S-Z* coordinates in the vertical), SELFE uses an efficient semi-implicit time stepping in conjunction with an Eulerian–Lagrangian method (ELM) to treat the advection. As a result, numerical stability is greatly enhanced and the errors from the "mode splitting" method are avoided; in fact, the only stability constraints are related to the explicit treatment of the horizontal viscosity and baroclinic pressure gradient, which are much milder than the stringent CFL condition. The default numerical scheme is 2nd-order accurate in space and time, but optional higher-order schemes have been developed as well (e.g., the dual kriging ELM proposed by *Le Roux et al.* [1997]). The model also incorporates wetting and drying in a natural way, and has been rigorously benchmarked for inundation problems [*Zhang and Baptista*, 2008b; *Zhang et al.*, 2011; *National Tsunami Hazard Mitigation Program*, 2012]. As an open-source community-supported model, SELFE has been well demonstrated to be accurate, efficient, robust and flexible, with a wide range of applications from general circulation [*Brovchenko et al.*, 2011], tsunami inundation [*Zhang et al.*, 2011], storm surge [*Bertin et al.*, 2012], ecology [*Rodrigues et al.*, 2009], oil spill [*Azevedo et al.*, 2009], and water quality studies.

[7] For realistic applications, phase averaged spectral wave models have the advantage of simulating sea state in an efficient manner [e.g., *Komen et al.*, 1994]. The wave model we adopt is the Wind Wave Model II (WWM-II), which is based on the source code by *Hsu et al.* [2005] but has since been overhauled by *Roland* [2009] in nearly all aspects of numerical schemes, physics, robustness and the efficiency to its present form (hence WWM-II). The WWM-II incorporates the framework of residual distribution schemes [see, e.g., *Abgrall*, 2006] within a hybrid fractional splitting method utilizing third order Ultimate Quickest schemes in spectral space, as also used by *Tolman* [1992] in the WAVEWATCH III (R) (WWIII) model, and robust and accurate integration of the source terms based on a multiple splitting technique using TVD-Runge Kutta schemes for shallow water wave breaking and bottom friction, dynamic integration of the triad interaction source term and semi-implicit integration of the deep water physics.

[8] The WWM-II model has previously been coupled to the SHYFEM (Shallow Water Finite Element Model) [*Umgiesser et al.*, 2004] and shown to be efficient in a variety of applications ranging from the Lagoon of Venice [*Ferrarin et al.*, 2008], the Adriatic Sea, the Gulf of Mexico [*Roland et al.*, 2009], and the South China Sea in order to investigate typhoon-induced waves in the vicinity of Taiwan [*Babanin et al.*, 2011].

[9] The numerical schemes for the advection of wave action in geographical space in WWM-II have also been successfully exported to the WWIII modeling framework and demonstrated to be accurate and efficient [*Ardhuin et al.*, 2009, 2010; *Ardhuin and Roland*, 2012].

[10] The work described here is a logical continuation from previous efforts, and further integrates WWM-II into a current model that is fully parallelized with a domain decomposition method such as SELFE. The wave and current models have been tightly coupled, with WWM-II written as a routine inside SELFE. In addition, the whole system has been parallelized via domain decomposition and Message Passing Interface (MPI); the two models also share same subdomains, but may use different time steps and different integration strategies, in order to maximize efficiency.

[11] At this stage of the development, the physical model for wave-current interaction is based on some relatively simple formulations of the underlying processes mentioned above. We show the capabilities as well as the limitations of this approach in different test cases and indicate in this way the clear necessity for the implementation of a consistent theoretical framework recently developed in this field [e.g., *Bennis et al.*, 2011].

[12] In the following sections, we present the details of each model and the coupling strategy, and carefully validate the coupled model with a series of progressively more challenging tests. In section 2, we briefly describe the formulations for each model and explain our methodology for model coupling. In section 3, the coupled model is then validated using one analytical and three laboratory tests, followed by a field test of Hurricane Isabel (2003). In all cases, the coupled model is shown to be able to qualitatively and quantitatively capture the important physical processes for wave-current interaction at a modest cost. We also highlight the challenges in accounting for wave effects in 3D current models. The main findings are summarized in section 4.

2. Description of the Wave-Current Model

2.1. Spectral Wave Model (WWM-II)

2.1.1. Governing Equations and Numerical Approach

[13] The Wave Action Equation (hereinafter WAE) is given as follows [e.g., *Komen et al.*, 1994]

$$\underbrace{\frac{\partial}{\partial t}N}_{\text{Change in Time}} + \underbrace{\nabla_{\mathbf{x}}\left(\dot{\boldsymbol{X}}N\right)}_{\text{Advection in horizontal space}} + \underbrace{\frac{\partial}{\partial\sigma}\left(\dot{\theta}N\right)+\frac{\partial}{\partial\theta}\left(\dot{\sigma}N\right)}_{\text{Advection in spectral space}} = \underbrace{S_{tot}}_{\text{Total Source Term}}, \tag{1}$$

where the Wave Action, which is invariant in slowly varying media [*Bretherton and Garrett*, 1968], is defined as

$$N_{(t,\boldsymbol{X},\sigma,\theta)} = \frac{E_{(t,\boldsymbol{X},\sigma,\theta)}}{\sigma}, \tag{2}$$

with E being the variance density of the sea level elevations, σ the relative wave frequency, and θ the wave direction. The advection velocities in the different phase spaces are given following the Geometric Optics Approximation [e.g., *Keller*, 1958]:

$$\dot{\boldsymbol{X}} = \boldsymbol{c}_{\boldsymbol{X}} = \frac{d\boldsymbol{X}}{dt} = \frac{d\omega}{dk} = \boldsymbol{c}_{\boldsymbol{g}} + \boldsymbol{U}_{A(\boldsymbol{k})} \tag{3a}$$

$$\dot{\theta} = c_\theta = \frac{1}{k}\frac{\partial\sigma}{\partial d}\frac{\partial d}{\partial m} + \boldsymbol{k}\cdot\frac{\partial \boldsymbol{U}_{A(\boldsymbol{k})}}{\partial s} \tag{3b}$$

$$\dot{\sigma} = c_\sigma = \frac{\partial\sigma}{\partial d}\left(\frac{\partial d}{\partial t} + \boldsymbol{U}_A\cdot\nabla_{\boldsymbol{X}} d\right) - c_g\boldsymbol{k}\frac{\partial \boldsymbol{U}_{A(\boldsymbol{k})}}{\partial s}. \tag{3c}$$

[14] Here **s** represents the coordinate along the wave propagation direction and **m** perpendicular to it. **X** is the Cartesian coordinate vector (x, y) in the geographical space, d is the water depth obtained from SELFE, **k** is the wave number vector (with $k = |\mathbf{k}|$), c_g the group velocity, ω is the absolute wave frequency, and $\nabla_{\boldsymbol{X}}$ is the gradient operator in the geographical space. The group velocity is calculated from the linear dispersion relation. The effective advection velocity U_A depends in general on the wave number vector of each wave component [*Andrews and McIntyre*, 1978a, 1978b, 1979], but in the present formulation this is approximated by the surface current.

[15] S_{tot} is the source function including the energy input due to wind (S_{in}), the nonlinear interaction in deep and shallow water (S_{nl4} and S_{nl3}), the energy dissipation in deep and shallow water due to whitecapping and wave breaking (S_{ds} and S_{br}) and the energy dissipation due to bottom friction (S_{bf}); we have

$$\frac{DN}{Dt} = S_{total} = S_{in} + S_{nl4} + S_{ds} + S_{nl3} + S_{br} + S_{bf}. \tag{4}$$

[16] WWM-II solves the WAE using the fractional step method as described by *Yanenko* [1971]. The fractional step method allows the splitting of the time dependent four dimensional problems in well-defined parts (equations (5a)–(5d)) for which dedicated numerical methods can be used in order to have a consistent and convergent numerical method [e.g., *Tolman*, 1992]:

$$\frac{\partial N^*}{\partial t} + \frac{\partial}{\partial\theta}(c_\theta N) = 0;\ \left[N^*_{(t=0)} = N_0\right] \text{ on } [0,\Delta t] \tag{5a}$$

$$\frac{\partial N^{**}}{\partial t} + \frac{\partial}{\partial\sigma}(c_\sigma N^*) = 0;\ \left[N^{**}_{(t=0)} = N^*_{(t=\Delta t)}\right] \text{ on } [0,\Delta t] \tag{5b}$$

$$\frac{\partial N^{***}}{\partial t} + \frac{\partial}{\partial x}(c_x N^{**}) + \frac{\partial}{\partial y}(c_y N^{**}) = 0;\ \left[N^{***}_{(t=0)} = N^{**}_{(t=\Delta t)}\right] \text{ on } [0,\Delta t] \tag{5c}$$

$$\frac{\partial N^{****}}{\partial t} = S_{(N^{**}),tot};\ \left[N^{****}_{(t=0)} = N^{***}_{(t=\Delta t)}\right] \text{ on } [0,\Delta t]. \tag{5d}$$

[17] WWM-II first solves the geographical part (equation (5c)) using the Residual Distribution (RD) Scheme, also known as "Fluctuation Splitting Scheme" [e.g., *Abgrall*, 2006]. The RD technique was first introduced by *Roe* [1982] and further developed and improved by other scientists (e.g., Abgrall, Deconinck, Roe and others). It borrows ideas from the FE and the FV framework, and as a result, compact schemes and accurate solutions can be achieved, that are carefully designed to obey most important constraints such as conservation property, positivity and linear preservation (2nd order in smooth flow); it can also be easily parallelized. A recent review on the history and future trends of RD-schemes is given by *Abgrall* [2006].

[18] In the 2nd step the spectral advection is treated by using Ultimate Quickest scheme [*Leonard*, 1991] in θ and σ space following the approach used in WWIII [*Tolman*, 1992]. The source terms are integrated in three separate fraction steps according to their time scales or nonlinearity. In the 1st step we integrate the dissipative terms in shallow water such as wave breaking and bottom friction and this is done using a TVD Runge–Kutta [e.g., *Gottlieb and Shu*, 1998] scheme of 3rd order without the necessity of an action limiter. Then we integrate the triad interaction source terms using a dynamic approach as suggested by *Tolman* [1992]. The reason for this procedure is that we found strong influence of the limiter on the integration of the triad interaction term, and so in the dynamic approach the limiter is applied only in the last iteration step. In the last step we integrate the deep water source terms using the well-known semi-implicit approach by *Hersbach and Janssen* [1999]. Our approach showed better convergence and confines the influence of the limiter to the deep water physics and the integration of the triad interactions, thus increasing the consistency of the whole numerical scheme. Previously, various limiters used in spectral wave models have rendered the numerical schemes inconsistent in that it is not at all stages a solution of the original equation system. According to the Lax-Wendroff equivalence theorem a convergence scheme must be consistent and stable. Therefore, reducing the influence of the limiter also greatly improves the convergence of the whole scheme.

[19] The implemented schemes in WWM-II are accurate; e.g., in the latest application of WWIII (which adopted the same numerical methods as WWM-II) using refined physics based on *Ardhuin et al.* [2009, 2010], the scatter indices (SCI's) are around 10% off the French Atlantic Coast.

2.1.2. Physical Formulation

[20] The nonlinear energy transfer in deep water (S_{nl4}), is approximated using the DIA (Discrete Interaction Approximation) following *Hasselmann and Hasselmann* [1985]. The Wind Input Term (see, e.g., *Janssen* [2001] for a review) and the Dissipation term (see, e.g., *Babanin et al.* [2011] for a review) in the WAE are undergoing continuous improvement and developments with the latest understanding of the underlying physical processes as well as more sophisticated measurements. Recently the wind input and dissipation function have been further improved [*Ardhuin et al.*, 2010] and validated on a remarkable data set in global and coastal

waters. The WWM-II has basically two main parameterizations for the wind input and dissipation: the 1st is used at the ECMWF (European Centre for Medium-range Weather Forecasts) and given in *Bidlot et al.* [2002], and a 2nd and more recent one that was proposed by *Ardhuin et al.* [2010]. In this study we have used the wind input and dissipation term as given by *Ardhuin et al.* [2010]; the shallow-water wave breaking formulation is based on the work of *Battjes and Janssen* [1978] and wave dissipation by bottom friction is modeled based on the results obtained from the JONSWAP experiment [*Hasselmann et al.*, 1973].

2.2. Hydrodynamic (Current) Model

[21] Since the original paper by *Zhang and Baptista* [2008a], SELFE has evolved into a comprehensive modeling system that can be configured in many different ways; e.g., hydrostatic or non-hydrostatic options; 3D bottom deformation as occurred during a seismically or landslide generated tsunamis; in 2D or 3D configuration; in Cartesian (i.e., map projection) or spherical coordinates; with several tracer transport modules (sediment, oil, ecology etc.). At the core of the SELFE model, the governing equations used in the hydrostatic, barotropic configuration of SELFE, which is used in this paper, are the 3D Reynolds averaged Navier–Stokes equations subject to the hydrostatic assumption and written in Cartesian coordinates:

$$\frac{D\mathbf{u}}{D\mathrm{t}} = \frac{\partial}{\partial z}\left(\nu\frac{\partial \mathbf{u}}{\partial z}\right) - g\nabla\eta + \mathbf{F}, \tag{6}$$

and the continuity equation:

$$\nabla\cdot\mathbf{u} + \frac{\partial w}{\partial z} = 0, \tag{7}$$

where D denotes the material derivative, $\mathbf{u} = (u, v)$ is the horizontal velocity, η is the surface elevation, $\nabla = (\partial/\partial x, \partial/\partial y)$ is the horizontal gradient operator, g is the gravitational acceleration, w is the vertical velocity, and the explicit term in equation (6) is given by

$$\mathbf{F} = \nabla\cdot(\mu\nabla\mathbf{u}) - f\mathbf{k}\times\mathbf{u} - \frac{1}{\rho_0}\nabla p_A + \alpha g\nabla\varphi + \mathbf{R}_s, \tag{8}$$

where $\mathbf{k}$ is a unit vector of the z-axis (pointing vertically upward), f is the Coriolis factor, α is the effective earth-elasticity factor, is the earth tidal potential, ν and μ are the vertical and horizontal eddy viscosities respectively that may be solved from turbulence closure schemes, ρ_0 is a reference water density, and p_A is the atmospheric pressure.

[22] The radiation stress term $\mathbf{R_s}$ is parameterized with different formulations [e.g., *Bennis and Ardhuin*, 2011; *Mellor*, 2011a, 2011b; *Bennis et al.*, 2011]. At this stage of model development we adopted the simplest radiation stress formulation originally proposed by *Longuet-Higgins and Stewart* [1962, 1964]:

$$\begin{cases} \mathbf{R}_s = \left(R_{sx}, R_{sy}\right) \\ R_{sx} = -\dfrac{1}{\rho_0 H}\dfrac{\partial S_{xx}}{\partial x} - \dfrac{1}{\rho_0 H}\dfrac{\partial S_{xy}}{\partial y} \\ R_{sy} = -\dfrac{1}{\rho_0 H}\dfrac{\partial S_{yy}}{\partial y} - \dfrac{1}{\rho_0 H}\dfrac{\partial S_{xy}}{\partial x} \end{cases} \tag{9}$$

with S_{xx}, S_{xy}, S_{yy} being the components of the radiation stress tensor, defined for an irregular wave spectrum according to *Battjes* [1974] as

$$S_{xy} = \int_0^{2\pi}\int_0^{\infty} N_{(\sigma,\theta)}\sigma\frac{c_{g(\sigma)}}{c_{p(\sigma)}}\sin(\theta)\cos(\theta)d\theta d\sigma$$

$$S_{xx} = \int_0^{2\pi}\int_0^{\infty} N_{(\sigma,\theta)}\cdot\sigma\cdot\left[\frac{c_{g(\sigma)}}{c_{p(\sigma)}}\left(\cos^2(\theta)+1\right) - \frac{1}{2}\right]d\theta d\sigma \tag{10}$$

$$S_{yy} = \int_0^{2\pi}\int_0^{\infty} N_{(\sigma,\theta)}\cdot\sigma\cdot\left[\frac{c_{g(\sigma)}}{c_{p(\sigma)}}\left(\sin^2(\theta)+1\right) - \frac{1}{2}\right]d\theta d\sigma$$

where $H = h + \eta$ is the total water depth, c_g and c_p are group and phase velocities. Note that the stress is uniform in the vertical dimension under this formulation.

[23] In addition, the total surface stress is estimated based on the actual sea state using the theory of *Janssen* [1991] and the extension made to it (e.g., sheltering of the young waves) in *Ardhuin et al.* [2010]. The total stress is passed to the current model in order to account for the surface stress and the enhanced mixing due to the wave breaking as expounded in *Craig and Banner* [1994].

[24] In shallow waters, the wave-induced bottom stress in the wave bottom boundary layer plays a crucial role in sediment transport and can thus significantly enhance bottom stress. The formulation we adopted here was originally proposed *by Grant and Madsen* [1979] (hereinafter GM79) and later modified by *Mathisen and Madsen* [1996] and implemented by *Zhang et al.* [2004]. It replaces the original bottom roughness (i.e., the sediment diameter or ripples height) with an apparent roughness z_{0b} as given below. The quadratic drag law used in SELFE is

$$\begin{aligned} &\boldsymbol{\tau}_b = \rho_0 C_D|\mathbf{u}|\mathbf{u} \\ &C_D = [\kappa/\log(z_b/z_0)]^2 \end{aligned} \tag{11}$$

where $\kappa = 0.4$ is the von Karman's constant, z_b is the height from the bottom to the top of the bottom computational cell, and z_0 is the bottom roughness related to the sediment grain size in the fixed bed without ripples.

[25] The maximum wave bottom stress is defined as

$$\tau_w = 0.5\rho_0 f_w U_w^2 \tag{12}$$

where U_w is the orbital velocity amplitude:

$$U_w^2 = \iint \frac{N_{(\sigma,\theta)}\sigma^3}{\sinh^2 kH}d\sigma d\theta. \tag{13}$$

[26] The combined wave-current friction factor f_w is a function of both the current and waves [*Zhang et al.*, 2004]:

$$\begin{cases} \gamma = \dfrac{|\boldsymbol{\tau}_b|}{\tau_w} \\ C_\gamma = \left(1 + 2\gamma|\cos\theta_w| + \gamma^2\right)^{1/2} \\ f_w = C_\gamma\exp\left[5.61\left(\dfrac{C_\gamma U_w}{30 z_0\omega}\right)^{-0.109} - 7.30\right] \end{cases}. \tag{14}$$

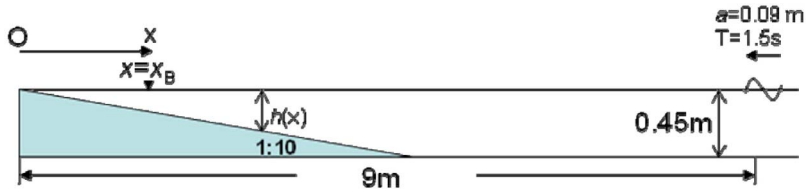

Figure 1. Sketch of sloping beach used in Longuet-Higgins and Stewart test.

[27] Equations (12) and (14) are solved iteratively for (γ, C_γ, τ_w) by first assuming $\gamma = 0$, $C_\gamma = 1$; convergence is usually achieved within a few iterations. After these quantities are found, the apparent roughness is given by

$$z_{0b} = \delta_{wc}\left(\frac{\delta_{wc}}{z_0}\right)^{-\sqrt{|\tau_b|/(C_\gamma \tau_w)}} \tag{15}$$

where the wave boundary layer thickness is given by

$$\delta_{wc} = \frac{\sqrt{\frac{C_\gamma \tau_w}{\rho_0}}}{\omega} \exp\left[2.96\left(\frac{C_\gamma U_w}{30 z_0 \omega}\right)^{-0.071} - 1.45\right]. \tag{16}$$

[28] The apparent roughness z_{0b} as given by equation (15) should then be used in place of z_0 in equation (11). The results shown in section 3.5 indicate that this apparent roughness can be much larger than z_0 even with modest waves inside estuaries.

[29] SELFE treats all terms in equation (6) semi-implicitly except for **F**; in other words the radiation stress terms are treated explicitly. The finite element formulation outlined in *Zhang and Baptista* [2008a] is applied to the additional radiation stress terms.

2.3. Model Coupling

[30] We first parallelized WWM-II using the same domain decomposition scheme as in SELFE. The use of same subdomains in the two models eliminates the need for interpolation and simplifies the exchange of information between the two models, resulting in greater efficiency. The WWM-II is then recast as a subroutine inside SELFE. Due to very different time stepping schemes used in the two models, the time steps used in the two models are kept different in order to take advantage of each model's efficiency, and information exchange between the two models takes place at a pre-specified interval. During the exchange, the surface elevation, wet/dry flags and velocity are passed from SELFE to WWM-II, and the calculated radiation stress, total surface stress, and the wave orbital velocity (needed in the Grant-Madsen formulation or GM79) are returned to SELFE. The ghost exchange routines in SELFE are also used inside WWM-II to exchange information in the ghost zones, e.g., for the wave action array. The robustness of both models has proved to be crucial for successful application of the coupled model to large field-scale tests.

3. Model Validation

[31] The model has been carefully tested using an analytical solution of wave setup on a linearly sloped beach profile and several laboratory experiments taken from the ONR Test Bed [*Ris et al.*, 2002]. Although mostly proposed to validate spectral wave models alone, this Test Bed contains many valuable cases for the validation of a fully coupled wave-current model as well.

[32] We have picked some of them for the validation of the present modeling system; in particular, we have compared wave-induced setup based on the laboratory experiment of *Boers* [1996], wave breaking and the eddy formation behind a submerged wave breaker based on the HISWA wave tank experiment of *Dingemans* [1987]; we have also investigated the performance of the coupled model in wave blocking conditions as measured in the laboratory by *Lai et al.* [1989]. In addition we have investigated the performance of the coupled model for many extra-tropical and tropical storm events, and here we will present the results for two hurricanes: Isabel (2003) making landfall at the U.S. east coast and Ivan (2004) in the Gulf of Mexico.

[33] The model settings have been set to the default parameterization from the literature and minimal tuning has been done. For the wave setup experiment of *Boers* [1996], we needed to modify the parameters for the wave breaking formulation in order to achieve similar decay rates as in the experiment.

3.1. Analytical Solution for the Wave Setup

[34] *Longuet-Higgins and Stewart* [1964] gave an analytical solution for wave set-up on a gently sloping beach. In this simple 1D steady state problem, the balance of forces is between the pressure gradient and the radiation stress:

$$g\frac{\partial \eta}{\partial x} = -\frac{1}{\rho_0 H}\frac{\partial E(2n-0.5)}{\partial x}. \tag{17}$$

where E is the total wave energy per unit surface area, and $n = \frac{1}{2}\left(1 + \frac{2kH}{\sinh 2kH}\right)$. The solution is given in two zones: inside and outside the surf zone (with the boundary defined as $x = x_B$, with x_B to be determined; see Figure 1). Outside the surf zone ($x \geq x_B$), we have

$$\eta = -\frac{a^2 k}{2\sinh 2kh}. \tag{18}$$

[35] In addition, the conservation of wave energy leads to

$$a^2 = \frac{n_0 k}{n k_0} a_0^2 \tag{19}$$

where the subscripts "0" denote the quantities related to the incident wave. Inside the surf zone ($x \leq x_B$), the wave amplitude is proportional to the local water depth:

$$a = \beta(h + \eta), \tag{20}$$

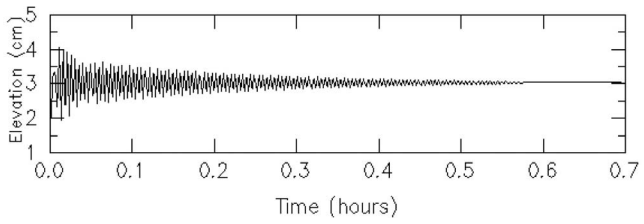

Figure 2. Convergence to steady state for elevation at x = 0.38 m (h = 0.038 m).

where $\beta = 0.41$ is a wave breaking constant as given by *Xia et al.* [2004]. If we assume a long-wave dispersion relation within this zone (i.e., $n = 1$), we then have

$$\eta = \frac{1}{1 + \frac{2}{3\beta^2}}(h_B - h) + \eta_B \tag{21}$$

where the subscripts "B" denote quantities at $x = x_B$.

[36] Matching the two solutions at $x = x_B$ leads to 4 equations for 4 unknowns (h_B, η_B, a_B, k_B): equations (18)–(21) plus the dispersion relation. If we assume a long-wave dispersion relation, the nonlinear equation system can be simplified to one equation for k_B:

$$k_B^{10} - \frac{8}{c_0}\left(1 + \frac{2}{\beta^2}\right)\hat{k}k_B^5 + \frac{16}{c_0}\hat{k}^4 = 0 \tag{22}$$

where $c_0 = a_0^2 n_0 / k_0, \hat{k} = \omega^2/g$. After k_B is solved from equation (22), the complete solution can be constructed within each zone. The solution, however, exhibits a sharp jump near the breaking point $x = x_B$ due to the use of the long-wave dispersion relation. If we hadn't assumed the long-wave dispersion relation in each zone, the unknowns can still be found by solving the original nonlinear equation system mentioned above. The latter approach is used here and the nonlinear equations are solved with an iterative method inside MATLAB.

[37] To test the coupled model, we impose a train of monochromatic wave with an amplitude of 9 cm and period of 1.5 s at the right-hand boundary for WWM-II (for SELFE, the elevation calculated from the analytical solution is imposed there); the initial elevations and velocities are both 0. The coupling time step (0.05 s) is chosen to be the same as the SELFE step, and the explicit *N*-scheme (a RD scheme) is used in WWM-II with sub time step being determined by the local CFL condition. The horizontal grid has a uniform resolution of 12.5 cm in x and 9 evenly distributed terrain-following σ levels are used in the vertical.; the symbol "σ" here refers to the terrain-following coordinates, and is not to be confused with the wave frequency used in equation (1) etc. As consistent with the analytical solution, no bottom friction was used. The total simulation time is 1 h in order to reach a steady state.

[38] A first check of the numerical model is on whether a steady state solution is reached as predicted by the analytical solution. It can be seen from Figure 2 that this is indeed the case for the surface elevation at a location close to the shoreline; it takes ~0.6 h for the initial high-frequency oscillations to dissipate before converging to a steady state, which is an indication of the monotonicity and consistency of the coupled model. The modeled steady state compares very well with the analytical solution for both wave height and wave induced set-up (Figure 3).

3.2. Wave Setup and Wave Breaking of *Boers* [1996]

[39] In the work of *Boers* [1996] depth-induced wave breaking and wave-induced set-up were examined under laboratory conditions. Boers investigated the evolution of random uni-directional wave trains in laboratory flume and measured wave spectra and surface evolution as the waves propagate toward a bar-trough profile as often found in natural conditions (see Figure 4). Observed wave spectra as well as wave-induced set-up are available at a large number of locations, making this a valuable test case for the validation of the coupled model. There are three cases for this test with different wave boundary conditions, given in terms of one dimensional wave spectra, and characterized by different mean wavelengths and wave heights.

[40] The main challenge in this test is related to the complex bottom profile and the inclusion of inundation zone; as a result, a steady state cannot be reached if either the current or the wave model has stability issues. Therefore the very fact that a steady state is reached in the coupled model, at a location very close to the shoreline, is a testament to the stability and robustness of both models (Figure 5).

[41] The coupled model is run on a uniform grid of 5 cm resolution in the horizontal and 9 evenly distributed σ levels in the vertical. The coupling time step of 0.1 s is again the same as SELFE's. The lab measured wave spectra and elevation time history are imposed at the boundary for WWM-II and SELFE respectively. Since no information is provided for the bottom roughness, we used a constant value of 1 mm. The WWM-II was set up to account for the quasi-resonant wave-wave interactions, bottom friction based on the JONSWAP formulation and wave breaking according to *Battjes and Janssen* [1978]. For the wave breaking formulation we had to reduce the default dissipation rate used in WWMII by ~50% to 0.5 and set a fixed maximum wave height to depth ratio of 0.8 in contrast to the default value of 0.73 in order to not over-dissipate wave energy due to breaking (see Figure 6). The near-resonant interactions had to be re-tuned and we reduced the coefficient suggested by *Eldeberky* [1996] and *Dingemans* [1998] from 1.0 to 0.5 in order to not overestimate the transfer of low frequency

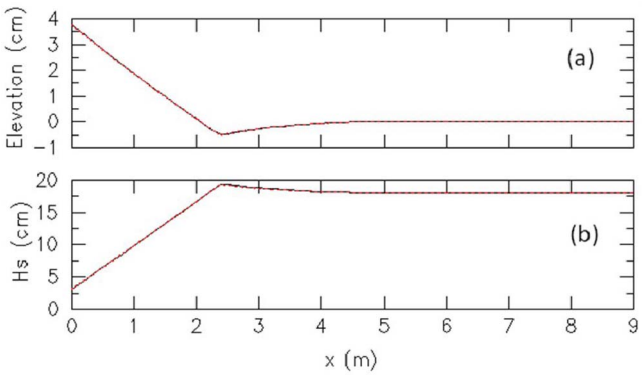

Figure 3. Comparison of analytical (dotted line) and numerical solutions (solid line) for (a) wave-induced set-up and (b) significant wave height.

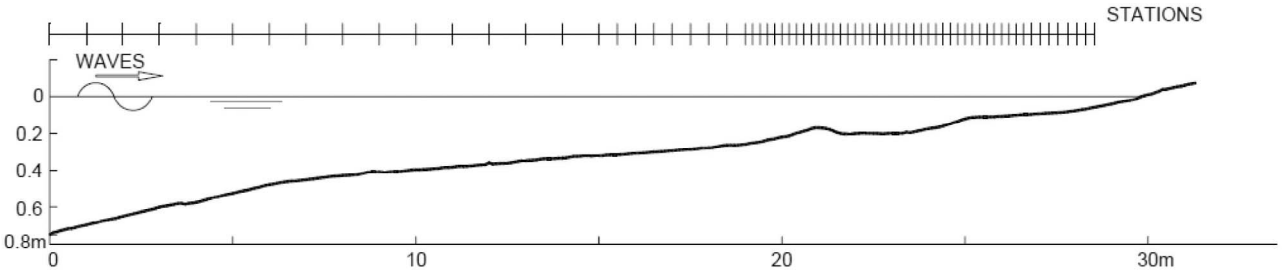

Figure 4. *Boers* [1996] lab set-up.

energy toward the higher harmonics (see Figure 6). Even though the downshift of the average period is well predicted on average, the model does not reproduce the downshifts in the vicinity of strong wave breaking dissipation (Figure 6). However, as discussed in *Dingemans* [1998], the approximation by Eldeberky is an approximation for a flat bottom and therefore the estimation of the near-resonant nonlinear transfer based on this approximation is not expected to be very accurate. Since the wave induced setup is sensitive to the spatial gradients of the wave spectrum, the overestimation of the wave set-up may be due to the fact that the model exaggerates the gradients of the total energy in the vicinity of the breaking point (Figure 6).

3.3. Wave Tank Experiment of *Dingemans* [1987]

[42] To test the coupled model in a 2D configuration, the ONR test L51 is used. The laboratory experiment of *Dingemans* [1987] was performed in a rectangular basin with flat bottom with a submerged breakwater (Figure 7). The two walls parallel to the x-axis are fully reflective and a target JONSWAP spectrum with a peak period of 1.25 s and height of 0.10 m was generated by the wave maker at the left-hand boundary while at the right-hand boundary a passive wave absorber was installed. The mean wave direction is along the x-axis with a directional spread of about 25°. The waves propagate across the breakwater with a significant loss of energy, generating a relatively large high-frequency spectral peak. The breaking waves also generate a mean circulation in the basin.

[43] The wave spectra derived from the lab data is imposed in the WWM-II at the left boundary, and a Neumann-type boundary are used on the north and south boundary of the basin while the east boundary condition is set to be fully absorbing. We used 72 directional and 36 frequency bins. As far as the current model is concerned, the basin is completely closed with fully reflective walls since the wave maker and the absorber operate at a higher frequency. We use an unstructured grid of ∼10 K nodes, with higher resolution (∼20 cm) near the breakwater (Figure 7b), and the same 9 σ levels as in the previous section. The coupling and SELFE time step is chosen to be 0.5 s, and the total simulation time is 2500 s, as a steady state is obtained after approximately 800 s.

[44] The modeled steady state surface velocity compares very well with the lab measurements both qualitatively and quantitatively (Figure 8). In particular the location of the eddy and the vorticity are both well simulated. The direction of the eddy indicates that the wave overtopping is the dominant process in this case as opposed to the diffraction/refraction effects as in the case shown in *Nicholson et al.* [1997].

[45] The modeled wave heights also compare well with the lab data, and capture the wave breaking process as waves propagate over the breakwater (Figure 9). Unsurprisingly, the largest error occurs on the down wave side of the breakwater. The errors at the 3 gauges nearest to the left boundary indicate the errors in the wave boundary condition given by the Web site.

[46] The lab data set also includes other types of measurements (e.g., vertical profiles of velocity) and will be further studied as the model incorporates consistent 3D formulations.

3.4. The Wave Blocking Experiment of *Lai et al.* [1989]

[47] The last laboratory experiment in this study investigates the capability of the coupled model to predict the wave decay in blocking conditions. The experiment conducted by *Lai et al.* [1989] investigated the evolution of uni-directional random waves running against an opposing current that was intensified by an underwater bar (Figure 10). The current velocity reaches a maximum of 24 cm/s over the bar, which is sufficient to block a large portion of the wave spectra imposed on the boundary. The waves propagate from left to right and are blocked at the toe of the bar.

[48] The grid used in this study has a uniform resolution of 2 m in cross-shore direction and 0.02 m in wave propagation direction, and SELFE uses six σ levels for the vertical discretization. The two models are coupled at a time step of 0.1 s, and the total simulation time is 10 min, which is sufficient to produce a convergent steady state solution (see Figure 11).

[49] The wave spectra at the 6 measurement stations, where gauge 1 is at the left boundary, are shown in Figure 12. The results are compared to the spectral balance as proposed by *Ardhuin et al.* [2010]. It can be clearly seen that the high-frequency part of the spectra that is blocked by

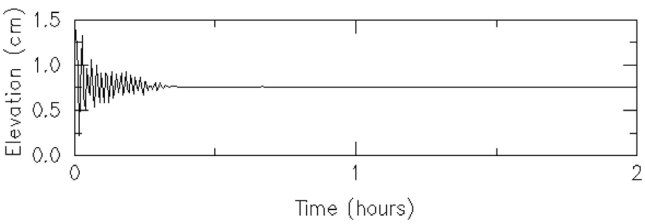

Figure 5. Convergence to a steady state for elevation for case A at x = 28.6 m.

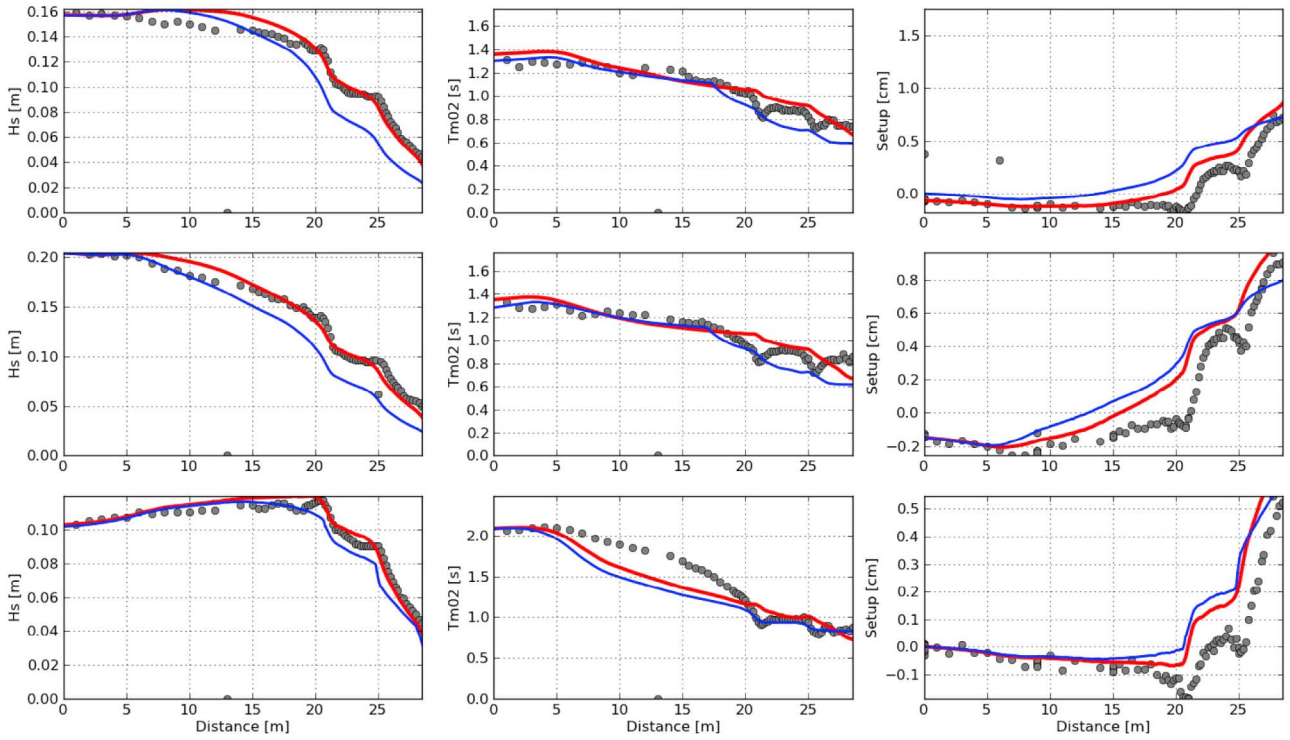

Figure 6. Comparison of wave heights, zero down crossing periods and wave induced setup for the three investigated cases between lab data (dots), model results using the default parameterization for triads and wave breaking (blue), and modified parameterization (red).

the counter current vanishes in the phase averaged model, while still present in the observation. In the vicinity of the spectral peak of the measurements it can be seen that the model is able to shift correctly the wave spectra in frequency space, and the peaks of the measured and modeled wave spectra are very close to each other. However, the dissipation of wave energy is strongly over-estimated. One reason for this may be due to the fact that near the blocking point part of the wave energy is reflected as shown in *Shyu and Phillips* [1990] and that the decay rate in blocking conditions is different due to the intense generation of turbulence.

[50] The most significant result of this comparison is that the fully coupled model was able to reach a convergent solution, and therefore it serves as a good basis for future investigation of possible new formulations that are able to improve the results under blocking conditions. This is important for practical application in tidal estuaries and other current dominated regions, where strong currents are present.

3.5. Hurricane Isabel (2003)

[51] Hurricane Isabel was the costliest and deadliest hurricane in the 2003 Atlantic hurricane season. It formed near

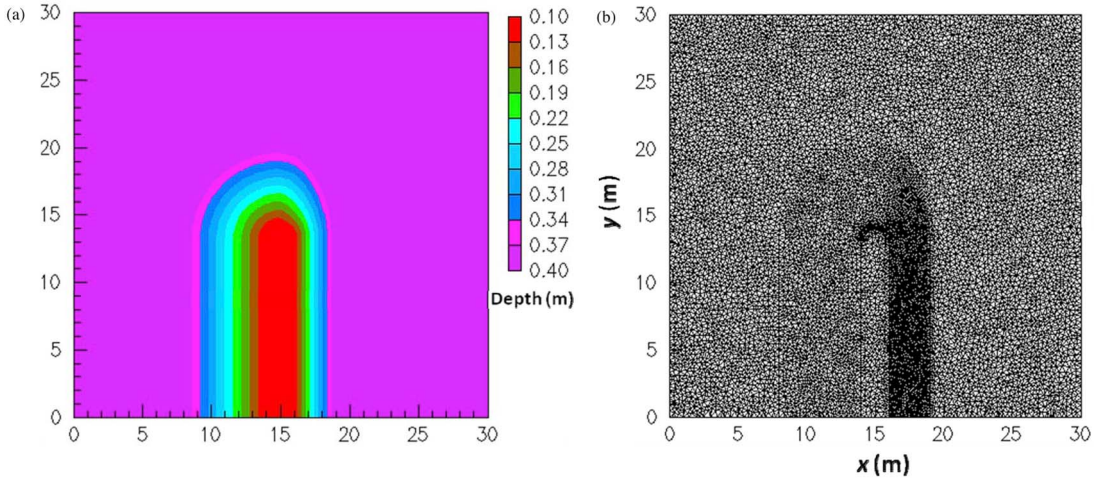

Figure 7. (a) L51 lab set-up; (b) unstructured grid.

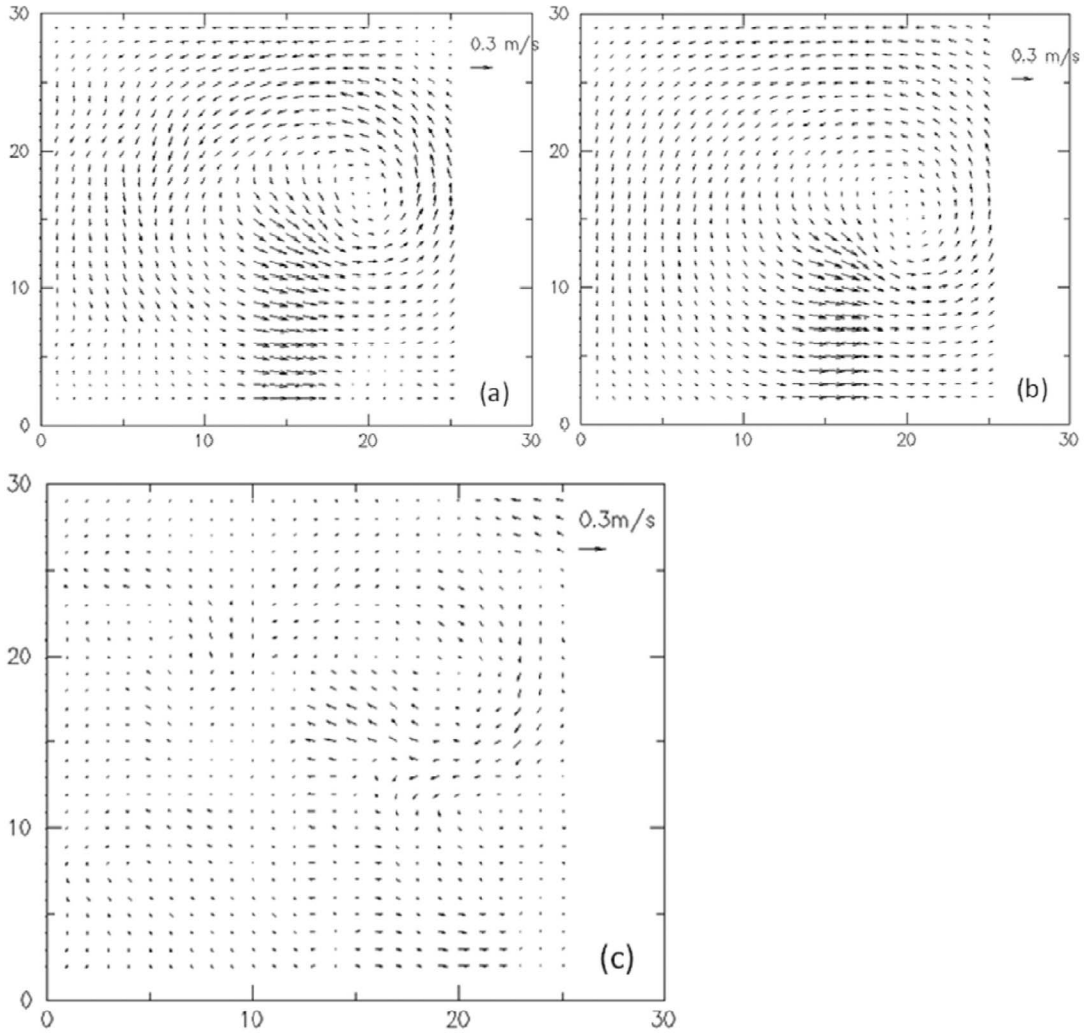

Figure 8. Comparison of wave-induced surface currents from (a) lab data, (b) model and (c) errors of Figures 8b and 8a. The global root-mean-square errors are 3 cm/s for *u*-component and 2 cm/s for *v*- component.

the Cape Verde Islands from a tropical wave on September 6 in the tropical Atlantic Ocean, moved northwestward, and steadily strengthened to reach peak winds of 165 mph on September 11. After fluctuating in intensity for four days, Isabel gradually weakened and made landfall on the Outer Banks of North Carolina with winds of 105 mph (47 m/s) on September 18. It quickly weakened over land and became an extratropical storm over western Pennsylvania the next day [*Hovis et al.*, 2004]. The total damage due to the storm is about $3 billion with 16 fatalities, mostly in North Carolina and Virginia.

[52] In order to accurately capture the wave dynamics from the deep ocean to nearshore, the model domain we used includes a large part of the mid-Atlantic Bight from Georgia to New Jersey, with higher resolution (~1 km) inside the Chesapeake Bay where extensive observation is available (Figure 13). The model grid we generated for this domain has ~26 K nodes in the horizontal and 34 *S* levels in the vertical (with stretching parameters $\theta_f = 6$ and $\theta_b = 0.5$). Note that S-coordinates are a family of generalized σ-coordinates proposed by *Song and Haidvogel* [1994]. The grid bathymetry was interpolated from a high-resolution DEM inside the Chesapeake Bay (NOAA/NGDC's Virginia Beach 1/3 arc-sec DEM; http://www.ngdc.noaa.gov/dem/squareCellGrid/download/423) and Coastal Relief Model (http://www.ngdc.noaa.gov/mgg/coastal/coastal.html) outside.

[53] The atmospheric forcing is based on the NARR (North American Regional Reanalysis; http://www.esrl.noaa.gov/psd/data/gridded/data.narr.pressure.html). The two models are coupled at a time step of 50 s.; and the smaller time step (by SELFE standard) was used to reduce splitting errors in WWM-II. The dual kriging ELM is used to obtain high-order accuracy for the momentum advection in SELFE. For WWM-II, we use 36 direction and 36 frequency bins, with the cut-off frequencies being 0.03 and 1 Hz. The wind growth and dissipation formulation is from *Ardhuin et al.* [2010]. At the offshore boundary, the integrated wave parameters have been prescribed based on the hindcast results produced by the WWIII from the IOWAGA project

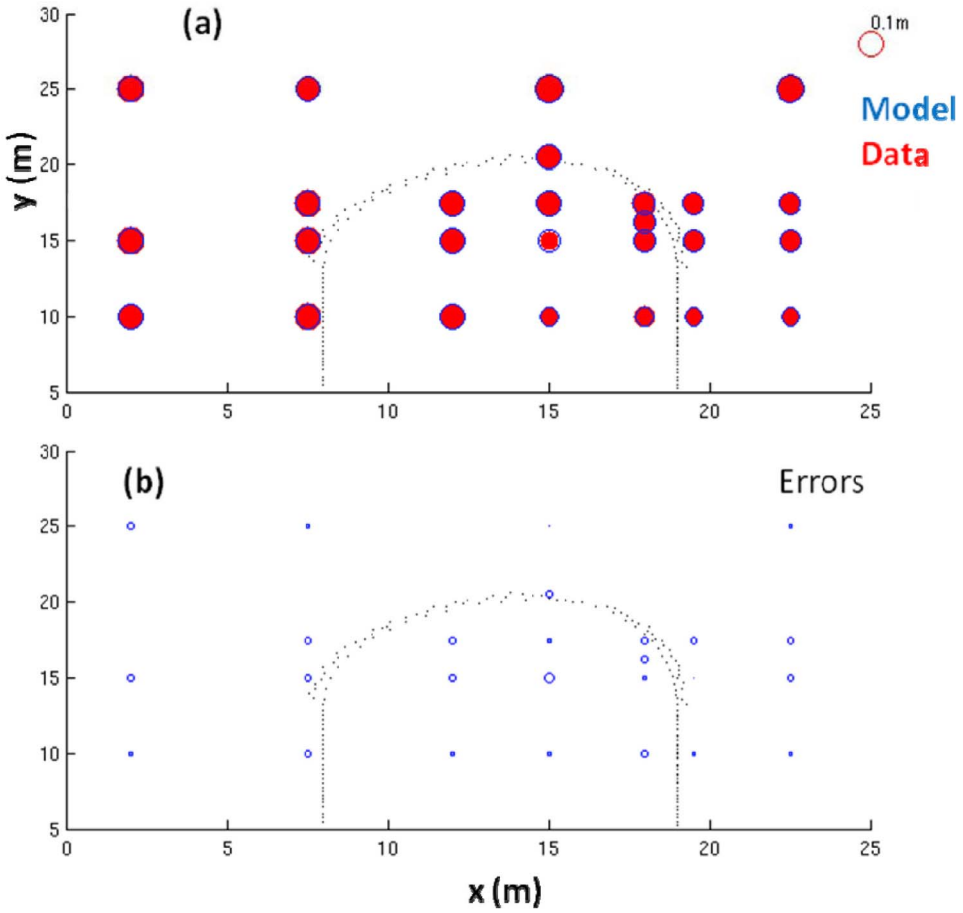

Figure 9. (a) Comparison of Hs at 26 stations between the lab data (squares) and model results (circles); the scale is shown at the upper right corner, and the dotted line is 0.4 m isobath. (b) Model errors. The root-mean-square error over the 26 stations is 7 mm.

(Integrated Ocean Waves for Geophysical and other Applications; http://wwz.ifremer.fr/iowaga).

[54] The fully coupled model runs ~24 times faster than real time on 48 CPUs of NASA's Pleiades cluster. To ascertain the effects from the waves, SELFE alone is run to simulate the storm surge without the wave effects. In addition, in order to elucidate the issues associated with the coupled 3D wave-current model, we conducted simulations with both 2D and 3D SELFE, with and without the wave effects.

[55] One of the major differences between 2D and 3D SELFE lies in the different bottom drag formulations used. After some calibration for tides, the initial distribution of the bottom roughness, used in the 3D model, is chosen as 1 mm outside the Chesapeake Bay and 0.1 mm inside; the modified Grant-Madson formulation is then used to dynamically adjust the wave-enhanced drag. As will be shown later, this initial distribution of bottom roughness will be quickly dwarfed by the increase caused by the GM79, and is therefore not a major factor here. For the 2D model, we use a *fixed* uniform Manning coefficient of 0.025, and the modified Grant-Madsen formulation is not applied therein.

[56] The modeled wave characteristics are found to be similar with the 2D and 3D models and compares well with the buoy data (Figure 14). Since Buoys 41008 and 44008 are close to the ocean boundary, the results there reflect the boundary condition from WWIII.

[57] The modeled surges, as predicted by the 2D models with and without waves, are shown in Figure 15 at lower Bay stations (we have also successfully simulated surges in the upper Bay with a grid that better represents the channels and shoals in that region. The upper Bay is also affected by other types of wave dynamics such as limited fetch, and is more sensitive to the atmospheric forcing. Therefore in this paper we focus on the lower Bay). The wave effects, mostly due to the radiation stress, account for up to 20 cm increase in the total set-up, which leads to a reduction of the average errors (averaged among all stations except Windmill) from 5.6% to 3.8% for the calculated surge heights.

[58] On the other hand, the addition of the 3D effects leads to some very interesting results. Without the waves (i.e., with SELFE alone), the addition of the vertical dimension from 2D to 3D SELFE generally results in a higher surge (Figure 16a) due to the Ekman dynamics included in the 3D model [*Kennedy et al.*, 2011]; similar results have also been obtained for Hurricane Ike in the Gulf of Mexico as well as many other tropical and extra-tropical storms (SURA, http://testbed.sura.org). The 3D results over-predicted the surge at all stations (Figure 16a). Adding the wave effects into the 3D model, however, leads to a net set-down (Figure 16a), which

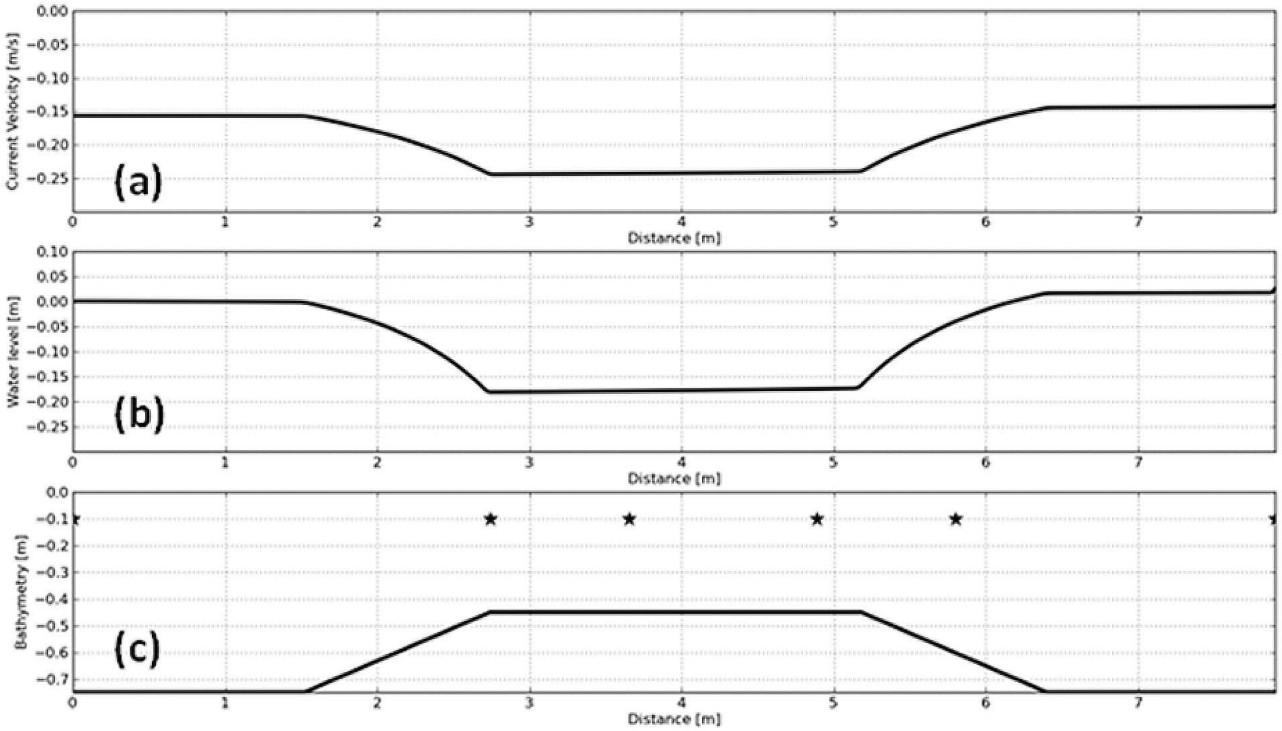

Figure 10. Along-channel profiles of the Lai *et al.* experiment (a) water level, (b) current velocity and (c) bathymetry. The stations 1–6 are marked with a star from left to right.

is contrary to the 2D results above. This is because inside the Bay the wave-enhanced bottom friction effects (calculated from the modified GM79 formulation) play a dominant role. Indeed, with the GM79 formulation taken out, the waves would have induced a higher surge (Figure 16a), most of which is attributed to the radiation stress. The apparent bottom roughness estimated by the GM79 formulation shows more than an order of magnitude increase from the initial 0.1 mm to several centimeters. Consequently, the current velocity is reduced (Figure 16b). The net set-down in the 3D models with waves has fortuitously reduced the errors in the surge heights from 8.2% to 6.1% due to the initial overprediction. It is also interesting to note that the 2D and 3D results with wave effects added are mostly close to each other (with the surge from the 3D model being slightly higher; Figure 16a).

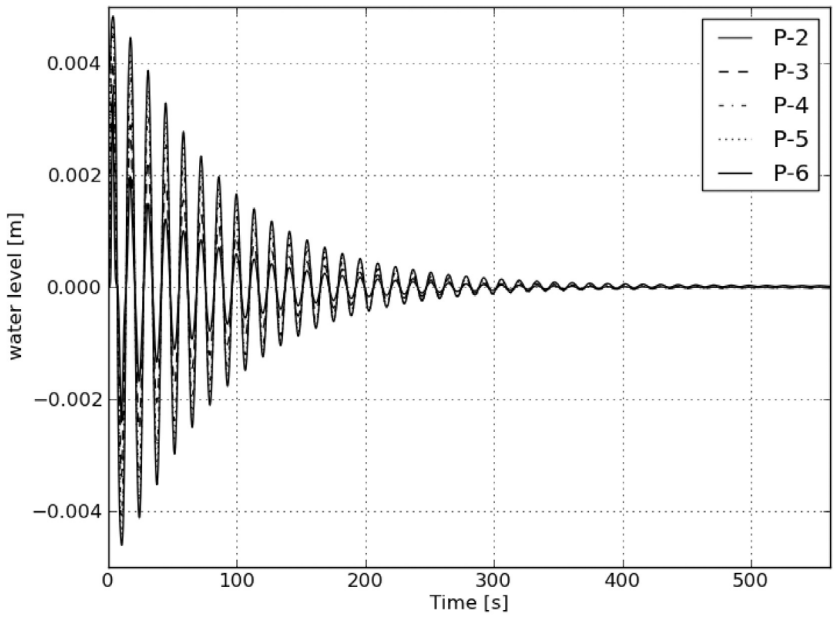

Figure 11. Convergence history of elevation along the 5 measurement locations.

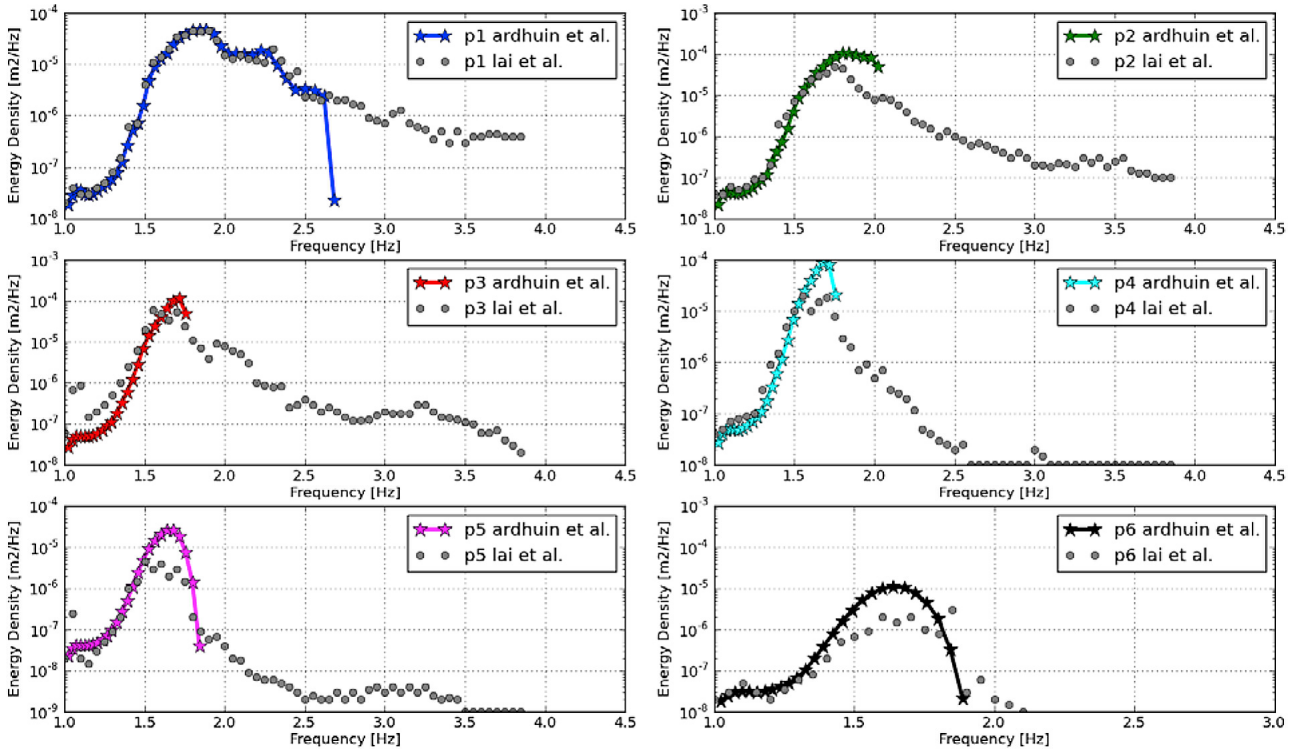

Figure 12. Measured (dots) and computed wave spectra (solid lines with stars) at the given location in a logarithmic scale.

[59] As explained in *Wolf* [2009], many different (and sometimes opposing) physical processes are at play in 3D, some of which are still under active research; e.g., wave-induced surface stress and turbulence and wave bottom friction (in shallow waters), and depth and current refraction of waves by surge water levels and currents. The results shown here further highlight the need to close the knowledge gap between the simple 2D and more "complete" (and presumably better) 3D wave-current models. It is our hope that the preliminary 3D results presented here will be further validated and improved after a more consistent framework such as that proposed in *Ardhuin et al.* [2008] is implemented in the model. At the moment, various components of the physical formulation in the model for radiation stress, surface stress and turbulence and wave bottom boundary layers are not entirely consistent as explained in *Bennis and Ardhuin* [2011]. To date, the only self-consistent equations were derived for the quasi-Eulerian velocity [*McWilliams et al.*, 2004; *Ardhuin et al.*, 2008]. Some practical applications with these have been performed by *Uchiyama et al.* [2010] and *Kumar et al.* [2012], but a comprehensive suite of tests to assess the skill of the 3D models under all conditions is still lacking.

[60] *Sheng et al.* [2010] also studied this event using a coupled wave-current model (with the current model being 3D), and showed that the addition of the waves effects has led to a higher (and more accurate) surge. Their conclusion is consistent with our 2D results, but not with the 3D results, where we have found a reduction of surge heights when the wave effects are added. The main differences between our and their 3D models include: (1) they used a table-lookup in the calculation of the wave-induced friction; (2) the underlying wave and current models used in their paper are based on structured grids, thus having limited ability to resolve the smaller features in the Bay that are important for wave propagation. Note that the Longuet-Higgins and Stewart formulation was also used by them.

4. Concluding Remarks

[61] The evolution of surface waves is influenced by the ambient currents on global and local scales. The current generation of spectral wave models is being continuously evaluated [e.g., *Bidlot et al.*, 2002] and these models are at a stage where it is not easy to make further improvements if the effect of currents is neglected, either on coastal or ocean scales. In the coastal zones surface waves induce coastal circulation and can have strong influence on the water levels, which are important for the coastal morphology and the coastal defense structures, and in return give a feed-back to the wave model and influence the wave evolution. Since the circulation model is far cheaper than the spectral wave model, we advocate the use of coupled wave current models in all scientific and engineering studies involving wave models. Neglecting the wave-current interactions is an assumption that can be hardly justified in tidal regions such as tidal seas, estuaries and wave dominated coasts.

[62] We have developed and validated a fully coupled wave-current interaction model based on a 3D hydrodynamic model (SELFE) and the spectral wave model (WWM-II), both implemented on unstructured grids, which makes the coupled model effective in multiscale applications without grid nesting. The two models are tightly coupled with same domain decomposition but with different time stepping

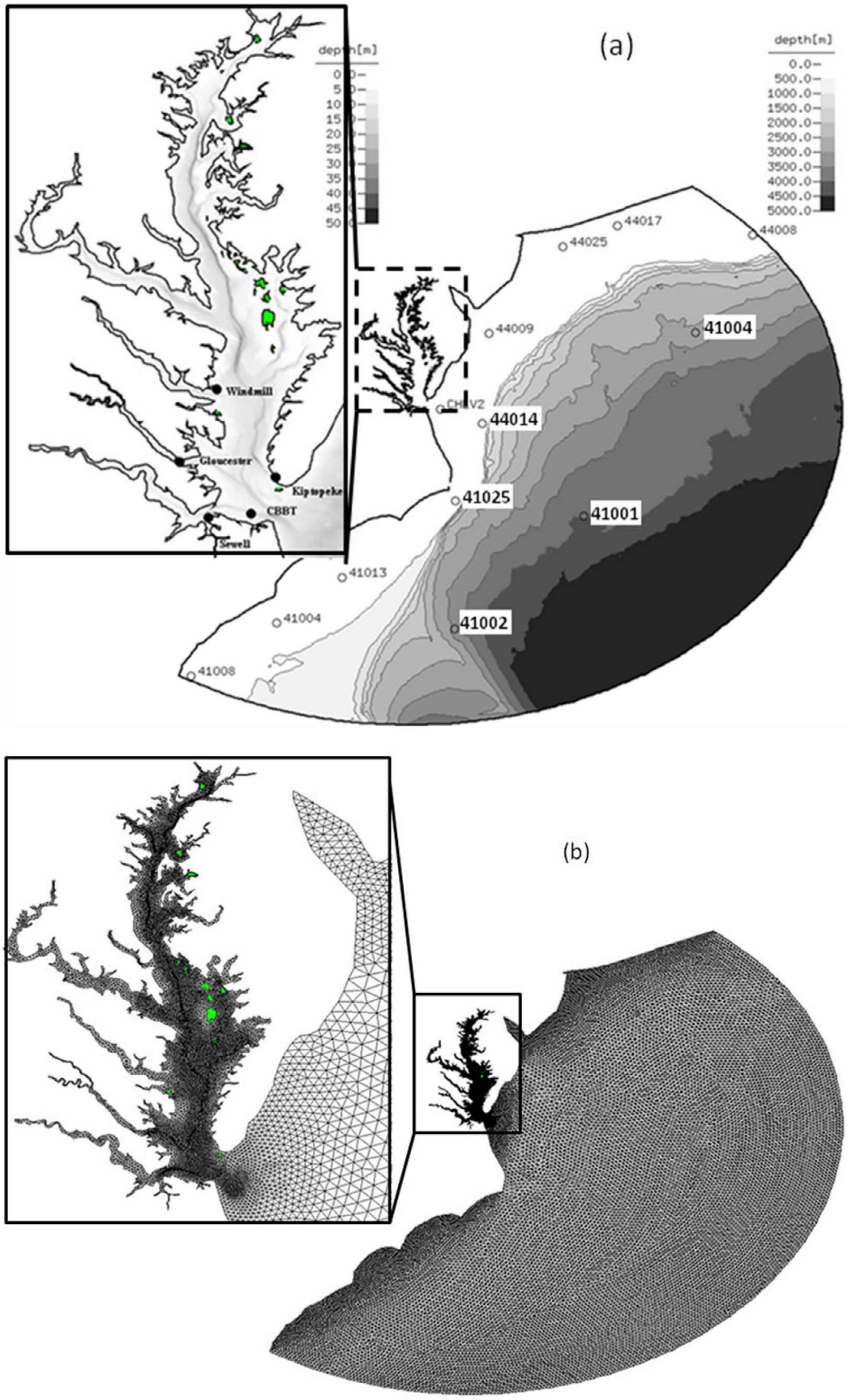

Figure 13. (a) Bathymetry in the computational domain with NDBC buoy locations and NOAA tide gauges; (b) numerical grid. The green patches are islands.

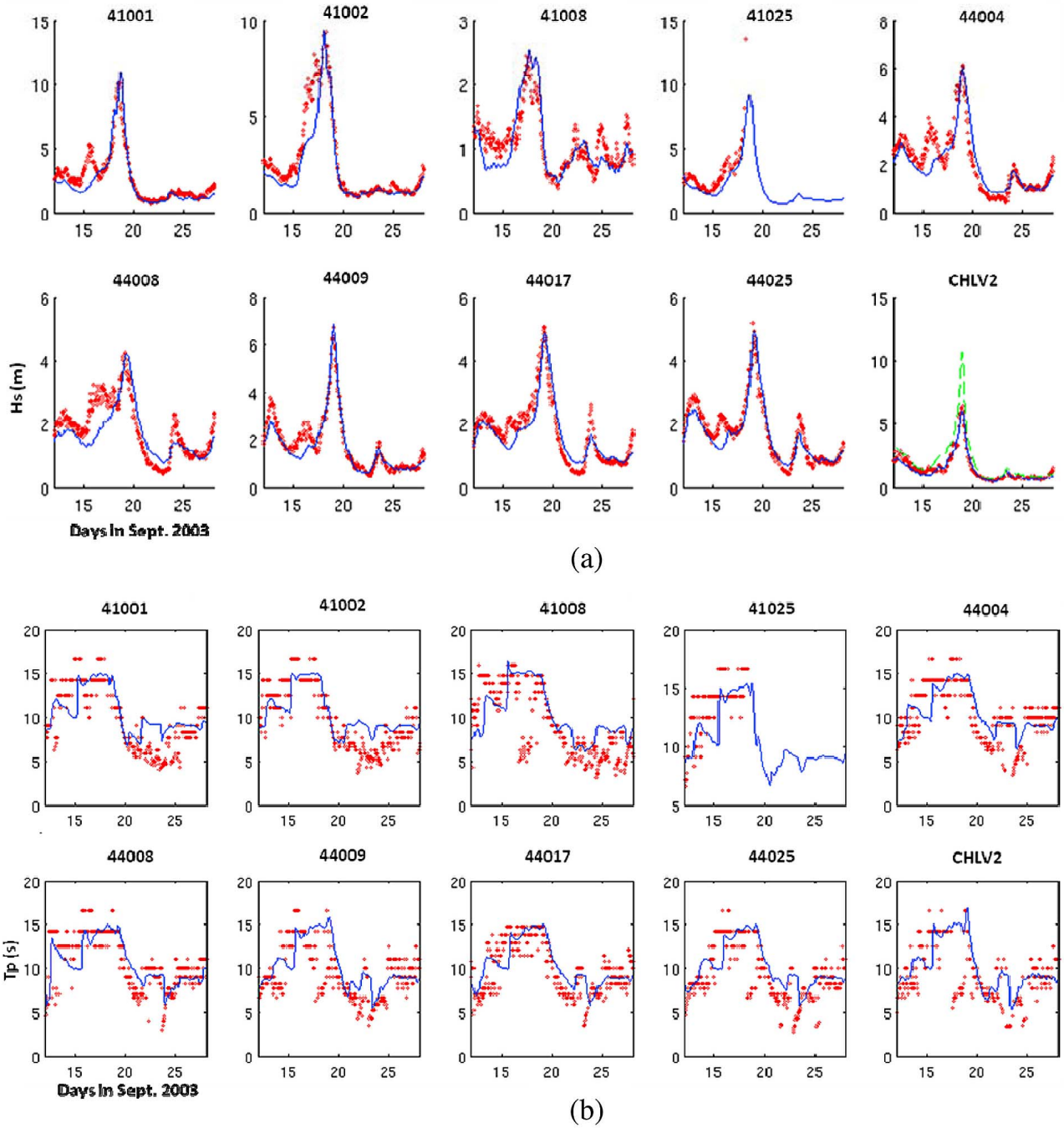

Figure 14. Comparison of (a) Hs and (b) Tp, between model (solid lines) and buoy observation (circles). The modeled Hs (with SELFE 3D) at Buoy 44014 (the dashed line) is overlaid with CHLV2 in the last panel of Figure 14a as well (note that the data are missing at 44014 during the hurricane period) to show the large dissipation of wave energy over the shelf as demonstrated in *Ardhuin et al.* [2003].

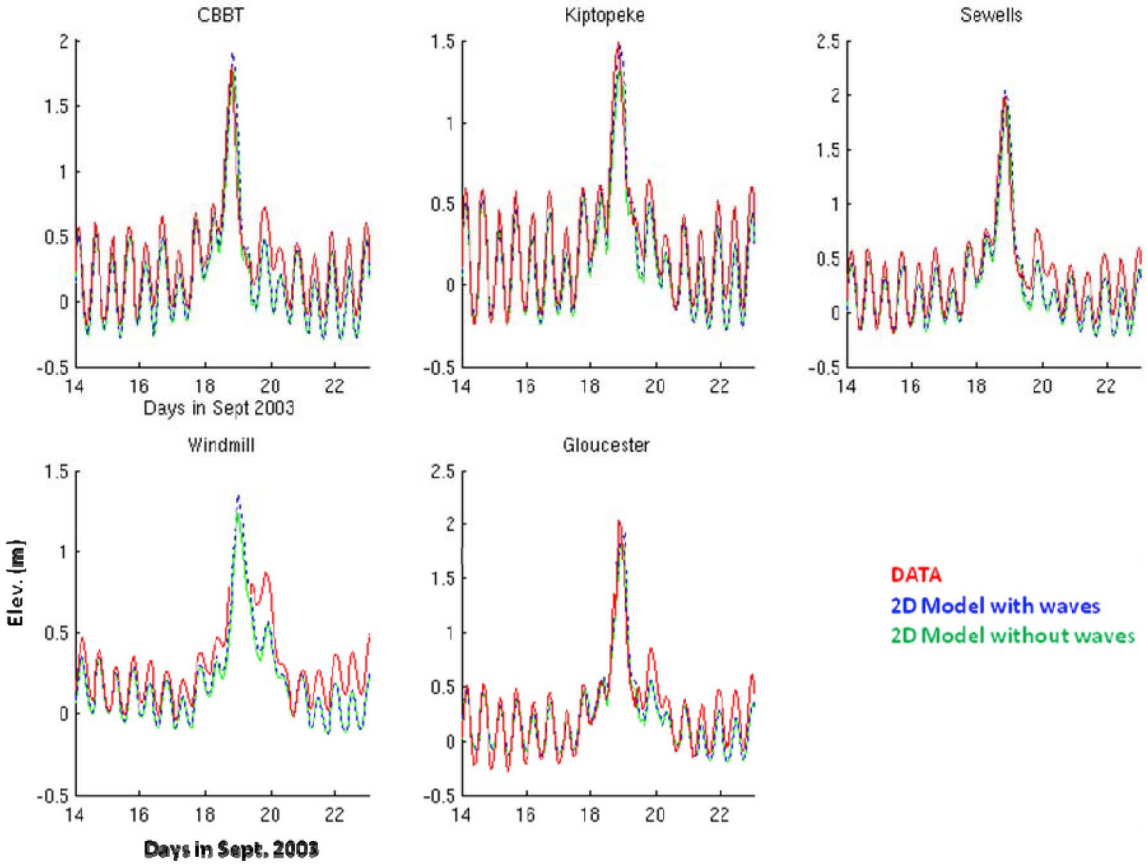

Figure 15. Comparison of elevations predicted from 2D models. Close-ups near the surge peaks can also be seen in Figure 16. Note that the observation has a gap near the maximum surge at Windmill.

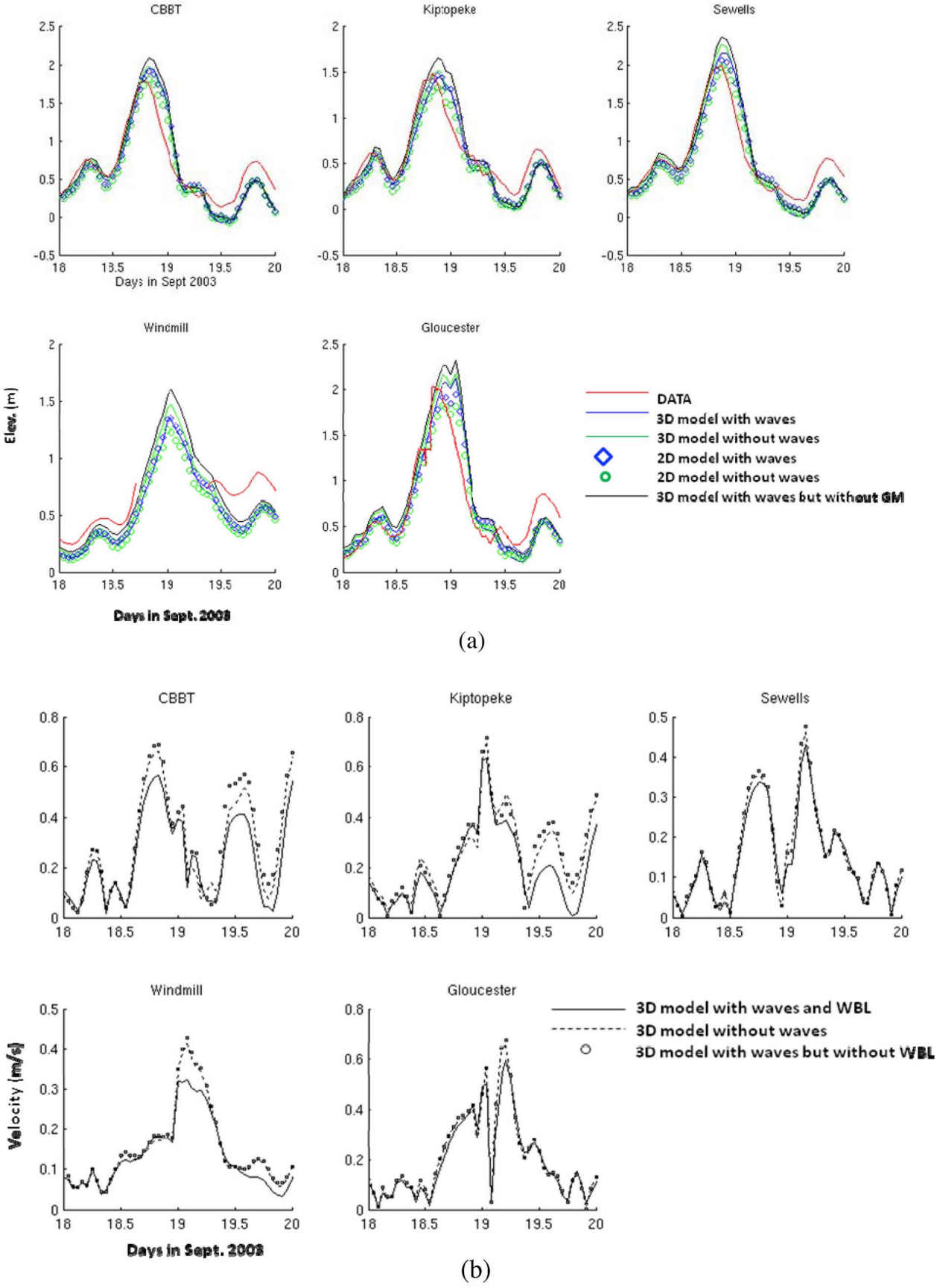

Figure 16. Comparison of (a) elevations predicted from 2D and 3D models; (b) depth-averaged velocity from 3D models. Note that the 3D model with waves but without WBL has the largest velocity.

schemes to ensure maximum efficiency and flexibility. The modeling framework serves as a basis for the future research into the important topic of wave-current interactions, the wave propagation in inhomogeneous media [e.g., *Liau et al.*, 2011; *Toledo et al.*, 2012] and the improvement and validation of the physical framework for phase-averaged surface wave models.

[63] The coupled model has been demonstrated to be accurate, robust, in addition to being efficient, through a series of stringent tests consisted of an analytical solution, three laboratory experiments and one cross-scale field test. From the numerical point of view the results presented are shown to be stable and consistent. In addition to the tests presented in this paper, we have also successfully applied the coupled model to other field scale tests, including in the context of the ongoing IOOS sponsored super-regional test bed for storm surge inundation.

[64] Our results for the 3D wave-current model also highlight the need to further understand the delicate inter-play of different and often opposing physical processes included in such complex nonlinear models, as the end results are not always easy to interpret. A consistent physical formulation for the wave-current interaction such as in *Ardhuin et al.* [2008] or *McWilliams et al.* [2004] will help shed more lights on the 3D results presented in this paper.

[65] **Acknowledgments.** This work was partly supported by the KFKI (German Coastal Engineering Research Council) and the German Federal Ministry of Education and Research (BMBF) (project 03KIS065). Some simulations shown in this paper were conducted on NASA's Pleiades and NSF/Teragrid's Ranger clusters, and we gratefully acknowledge their generous support. The authors are grateful to Peter Janssen, who made the performance evaluation at c1a/c1b at ECMWF possible.

References

Abgrall, R. (2006), Residual distribution schemes: Current status and future trends, *Comput. Fluids*, *35*(7), 641–669, doi:10.1016/j.compfluid.2005.01.007.

Andrews, D. G., and M. E. McIntyre (1978a), On wave-action and its relatives, *J. Fluid Mech.*, *89*, 647–664.

Andrews, D. G. and M. E. McIntyre (1978b), An exact theory of nonlinear waves on a Lagrangian-mean flow, *J. Fluid Mech.*, *89*, 609–646.

Andrews, D. G., and M. E. McIntyre (1979), Corrigendum: On wave-action and its relatives, *J. Fluid Mech.*, *95*, 796.

Ardhuin, F., and A. Roland (2012), Coastal wave reflection, directional spread, and seismo-acoustic noise sources, *J. Geophys. Res.*, *117*, C00J20, doi:10.1029/2011JC007832.

Ardhuin, F., W. C. O'Reiley, T. H. C. Herbers, and P. F. Jessen (2003), Swell transformation across the continental shelf. Part I: Attenuation and directional broadening, *J. Phys. Oceanogr.*, *33*, 1921–1939, doi:10.1175/1520-0485(2003)033<1921:STATCS>2.0.CO;2.

Ardhuin, F., N. Rascle, and K. A. Belibassakis (2008) Explicit wave-averaged primitive equations using a generalized Lagrangian mean, *Ocean Modell.*, *20*, 35–60.

Ardhuin, F., L. Marié, N. Rascle, P. Forget, and A. Roland (2009), Observation and estimation of Lagrangian, Stokes, and Eulerian currents induced by wind and waves at the sea surface, *J. Phys. Oceanogr.*, *39*(11), 2820–2838, doi:10.1175/2009JPO4169.1.

Ardhuin, F., et al. (2010), Semiempirical dissipation source functions for ocean waves. Part I: Definition, calibration, and validation, *J. Phys. Oceanogr.*, *40*(9), 1917–1941, doi:10.1175/2010JPO4324.1.

Azevedo, A., A. Oliveira, A. B. Fortunato, and X. Bertin (2009), Application of an Eulerian–Lagrangian oil spill modeling system to the Prestige accident: Trajectory analysis, *J. Coastal Res.*, *56*, 777–781.

Babanin, A. V., T.-W. Hsu, A. Roland, S.-H. Ou, D.-J. Doong, and C. C. Kao (2011), Spectral wave modelling of Typhoon Krosa, *Nat. Hazards Earth Syst. Sci.*, *11*, 501–511, doi:10.5194/nhess-11-501-2011.

Battjes, J. A. (1974), Computation of set-up, longshore currents, run-up, and overtopping due to wind-generated waves, *Rep. 74–2*, Comm. on Hydraul., Dep. of Civ. Eng., Delft Univ. of Technol., Delft, Netherlands.

Battjes, J. A., and J. Janssen (1978), Energy loss and set-up due to breaking of random waves, paper presented at 16th International Conference on Coastal Engineering, Coastal Eng. Res. Counc., Hamburg, Germany.

Bennis, A.-C., and F. Ardhuin (2011), Comments on "The depth-dependent current and wave interaction equations: A revision", *J. Phys. Oceanogr.*, *41*(10), 2008–2012, doi:10.1175/JPO-D-11-055.1.

Bennis, A.-C., F. Ardhuin, and F. Dumas (2011), On the coupling of wave and three-dimensional circulation models: Choice of theoretical framework, practical implementation and adiabatic tests, *Ocean Modell.*, *40*(3–4), 260–272, doi:10.1016/j.ocemod.2011.09.003.

Bertin, X., A. Oliveira, and A. B. Fortunato (2009), Simulating morphodynamics with unstructured grids: Description and validation of a modeling system for coastal applications, *Ocean Modell.*, *28*(1–3), 75–87, doi:10.1016/j.ocemod.2008.11.001.

Bertin, X., N. Bruneau, J.-F. Breilh, A. B. Fortunato, and M. Karpytchev (2012), Importance of wave age and resonance in storm surges: The case Xynthia, Bay of Biscay, *Ocean Modell.*, *42*, 16–30, doi:10.1016/j.ocemod.2011.11.001.

Bidlot, J. R., J. H. Damian, A. W. Paul, L. Roop, and S. C. Hsuan (2002), Intercomparison of the performance of operational ocean wave forecasting systems with buoy data, *Weather Forecast.*, *17*, 287–310, doi:10.1175/1520-0434(2002)017<0287:IOTPOO>2.0.CO;2.

Boers, M. (1996), Simulation of a surf zone with a barred beach; report 1: Wave heights and wave breaking. Communications on hydraulic and geotechnical engineering, Delft Univ. of Technol., Delft, Netherlands.

Bowen, A. J. (1969), The generation of longshore currents on a plane beach, *J. Mar. Res.*, *27*, 206–215.

Bretherton, F. P., and C. J. R. Garrett (1968), Wavetrains in inhomogeneous moving media, *Proc. R. Soc. London A*, *302*(1471), 529–554, doi:10.1098/rspa.1968.0034.

Brovchenko, I., V. Maderich, and K. Terletska (2011), Numerical simulations of 3D structure of currents in the region of deep canyons on the east coast of the Black Sea, *Int. J. Comput. Civ. Struct. Eng.*, *7*(2), 47–53.

Burla, M., A. M. Baptista, Y. Zhang, and S. Frolov (2010), Seasonal and interannual variability of the Columbia River plume: A perspective enabled by multiyear simulation databases, *J. Geophys. Res.*, *115*, C00B16, doi:10.1029/2008JC004964.

Craig, P. D., and M. L. Banner (1994), Modeling wave-enhanced turbulence in the ocean surface layer, *J. Phys. Oceanogr.*, *24*(12), 2546–2559, doi:10.1175/1520-0485(1994)024<2546:MWETIT>2.0.CO;2.

Dietrich, J. C., M. Zijlema, J. J. Westerink, L. H. Holthuijsen, C. Dawson, R. A. Luettich Jr., R. E. Jensen, J. M. Smith, G. S. Stelling, and G. W. Stone (2011), Modeling hurricane waves and storm surge using integrally coupled, scalable computations, *Coastal Eng.*, *58*(1), 45–65, doi:10.1016/j.coastaleng.2010.08.001.

Dingemans, M. W. (1987), Verification of numerical wave propagation models with laboratory measurements; HISWA verification in the directional wave basin, *Rep. H228*, 400 pp., Delft Hydraul., Delft, Netherlands.

Dingemans, M. W. (1998), A review of the physical formulations in SWAN, *Rep. H3306*, Delft Hydraul., Delft, Netherlands.

Eldeberky, Y. (1996), Nonlinear transformation of wave spectra in the nearshore zone, PhD thesis, Deft Univ. of Technol., Delft, Netherlands.

Ferrarin, C., G. Umgiesser, A. Cucco, T.-W. Hsu, A. Roland, and C. L. Amos (2008), Development and validation of a finite element morphological model for shallow water basins, *Coastal Eng.*, *55*(9), 716–731, doi:10.1016/j.coastaleng.2008.02.016.

Gottlieb, S., and C.-W. Shu (1998), Total variation diminishing Runge–Kutta schemes, *Math. Comput.*, *67*, 73–86, doi:10.1090/S0025-5718-98-00913-2.

Grant, W. D., and O. S. Madsen (1979), Combined wave and current interaction with a rough bottom, *J. Geophys. Res.*, *84*(C4), 1797–1808, doi:10.1029/JC084iC04p01797.

Hasselmann, K., T. P. Barnett, E. Bouws, D. E. Carlson, and P. Hasselmann (1973), Measurements of wind-wave growth and swell decay during the Joint North Sea Wave Project (JONSWAP), *Dtsch. Hydrogr. Z.*, *8*(12), 95–102.

Hasselmann, S., and K. Hasselmann (1985), Computations and parameterizations of the nonlinear energy transfer in a gravity-wave spectrum. Part I: A new method for efficient computations of the exact nonlinear transfer integral, *J. Phys. Oceanogr.*, *15*(11), 1369–1377, doi:10.1175/1520-0485(1985)015<1369:CAPOTN>2.0.CO;2.

Hersbach, H., and P. A. E. M. Janssen (1999), Improvement of the short-fetch behavior in the Wave Ocean Model (WAM), *J. Atmos. Oceanic Technol.*, *16*(7), 884–892, doi:10.1175/1520-0426(1999)016<0884:IOTSFB>2.0.CO;2.

Hovis, J., W. Popovich, C. Zervas, J. Hubbard, H. H. Shih, and P. Stone (2004), Effects of Hurricane Isabel on water levels, *NOAA Tech. Rep.*, *NOS CO-OPS 040*, 120 pp.

Hsu, T.-W., S.-H. Ou, and J.-M. Liau (2005), Hindcasting nearshore wind waves using a FEM code for SWAN, *Coastal Eng.*, *52*(2), 177–195, doi:10.1016/j.coastaleng.2004.11.005.

Janssen, P. (1989), Wave-induced stress and the drag of air flow over sea waves, *J. Phys. Oceanogr.*, *19*(6), 745–754, doi:10.1175/1520-0485(1989)019<0745:WISATD>2.0.CO;2.

Janssen, P. (1991), Quasi-linear theory of wind-wave generation applied to wave forecasting, *J. Phys. Oceanogr.*, *21*(11), 1631–1642, doi:10.1175/1520-0485(1991)021<1631:QLTOWW>2.0.CO;2.

Janssen, P. A. E. M. (2001), Reply, *J. Phys. Oceanogr.*, *31*(8), 2537–2544, doi:10.1175/1520-0485(2001)031<2537:R>2.0.CO;2.

Keller, J. B. (1958), Surface waves on water of non-uniform depth, *J. Fluid Mech.*, *4*(6), 607–614, doi:10.1017/S0022112058000690.

Kennedy, A. F., U. Gravois, B. C. Zachry, J. J. Westerink, M. E. Hope, J. C. Dietrich, M. D. Powell, A. T. Cox, R. A. Luettich Jr., and R. G. Dean (2011), Origin of the Hurricane Ike forerunner surge, *Geophys. Res. Lett.*, *38*, L08608, doi:10.1029/2011GL047090.

Komen, G. J., L. Cavaleri, M. Donelan, K. Hasselmann, S. Hasselmann, and P. A. E. M. Janssen (1994), *Dynamics and Modelling of Ocean Waves*, 532 pp., Cambridge Univ. Press, Cambridge, U. K., doi:10.1017/CBO9780511628955.

Kumar, N., G. Voulgaris, J. C. Warner, and M. Olaberrieta (2012), Implementation of the vortex force formalism in the Coupled Ocean–atmosphere-Wave-Sediment Transport (COAWST) modeling system for inner shelf and surf zone applications, *Ocean Modell.*, *47*, 65–95, doi:10.1016/j.ocemod.2012.01.003.

Lai, R. J., S. R. Long, and N. E. Huang (1989), Laboratory studies of wave-current interaction: Kinematics of the strong interaction, *J. Geophys. Res.*, *94*(C11), 16,201–16,214, doi:10.1029/JC094iC11p16201.

Le Roux, D. Y., C. A. Lin, and A. Staniforth (1997), An accurate interpolating scheme for semi-Lagrangian advection on an unstructured mesh for ocean modelling, *Tellus, Ser. A*, *49*(1), 119–138, doi:10.1034/j.1600-0870.1997.00009.x.

Leonard, B. P. (1991), The ultimate conservative difference scheme applied to unsteady one–dimensional advection, *Comput. Methods Appl. Mech. Eng.*, *88*(1), 17–74, doi:10.1016/0045-7825(91)90232-U.

Liau, J.-M., A. Roland, T.-W. Hsu, S.-H. Ou, and Y.-T. Li (2011), Wave refraction-diffraction effect in the wind wave model WWM, *Coastal Eng.*, *58*, 429–443, doi:10.1016/j.coastaleng.2011.01.002.

Longuet-Higgins, M. S., and R. W. Stewart (1962), Radiation stress and mass transport in gravity waves, with application to 'surf beats', *J. Fluid Mech.*, *13*(04), 481–504, doi:10.1017/S0022112062000877.

Longuet-Higgins, M. S., and R. W. Stewart (1963), A note on wave set-up, *J. Mar. Res.*, *21*, 4–10.

Longuet-Higgins, M. S., and R. W. Stewart (1964), Radiation stresses in water waves; a physical discussion, with applications, *Deep Sea Res. Oceanogr. Abstr.*, *11*(4), 529–562, doi:10.1016/0011-7471(64)90001-4.

Mathisen, P. P., and O. S. Madsen (1996), Waves and currents over a fixed rippled bed: 2. Bottom and apparent roughness experienced by currents in the presence of waves, *J. Geophys. Res.*, *101*(C7), 16,543–16,550, doi:10.1029/96JC00955.

McWilliams, J. C., J. M. Restrepo, and E. M. Lane (2004), An asymptotic theory for the interaction of waves and currents in coastal waters, *J. Fluid Mech.*, *511*, 135–178, doi:10.1017/S0022112004009358.

Mellor, G. (2011a), Reply, *J. Phys. Oceanogr.*, *41*(10), 2013–2015, doi:10.1175/JPO-D-11-071.1.

Mellor, G. (2011b), Wave radiation stress, *Ocean Dyn.*, *61*(5), 563–568, doi:10.1007/s10236-010-0359-2.

National Tsunami Hazard Mitigation Program (2012), NTHMP MMS Tsunami Inundation Model Validation Workshop, Galveston, April 2011, internal report, NOAA, Washington, D. C., in press.

Nicholson, J., I. Broker, J. A. Roelvink, D. Price, J. M. Tanguy, and L. Moreno (1997), Intercomparison of coastal area morphodynamic models, *Coastal Eng.*, *31*(1–4), 97–123, doi:10.1016/S0378-3839(96)00054-3.

Ris, R., et al. (2002), The ONR test bed for coastal and oceanic wave models, *Rep. WL 3627*, WL Delft, Delft, Netherlands.

Rodrigues, M., A. Oliveira, H. Queiroga, A. B. Fortunato, and Y. Zhang (2009), Three-dimensional modeling of the lower trophic levels in the Ria de Aveiro (Portugal), *Ecol. Modell.*, *220*(9–10), 1274–1290, doi:10.1016/j.ecolmodel.2009.02.002.

Roe, P. L. (1982), Numerical modelling of shockwaves and other discontinuities, in *Numerical Methods in Aeronautical Fluid Dynamics*, edited by P. L. Roe, pp. 1–43, Academic, London.

Roland, A. (2009), Development of WWM II: Spectral wave modeling on unstructured meshes, PhD thesis, Inst. of Hydraul. and Water Resour. Eng., Tech. Univ. Darmstadt, Darmstadt, Germany.

Roland, A., A. Cucco, C. Ferrarin, T.-W. Hsu, J.-M. Liau, S.-H. Ou, G. Umgiesser, and U. Zanke (2009), On the development and verification of a 2-D coupled wave-current model on unstructured meshes, *J. Mar. Syst.*, *78*, S244–S254.

Sheng, Y. P., V. Alymov, and V. A. Paramygin (2010), Simulation of storm surge, wave, currents, and inundation in the Outer Banks and Chesapeake Bay during Hurricane Isabel in 2003: The importance of waves, *J. Geophys. Res.*, *115*, C04008, doi:10.1029/2009JC005402.

Shyu, J.-H., and O. M. Phillips (1990), The blockage of gravity and capillary waves by longer waves and currents, *J. Fluid Mech.*, *217*, 115–141, doi:10.1017/S0022112090000659.

Song, Y., and D. Haidvogel (1994), A semi-implicit ocean circulation model using a generalized topography-following coordinate system, *J. Comput. Phys.*, *115*, 228–244, doi:10.1006/jcph.1994.1189.

Takaya, Y., J.-R. Bidlot, A. C. M. Beljaars, and P. A. E. M. Janssen (2010), Refinement to a prognostic scheme of skin sea surface temperature, *J. Geophys. Res.*, *115*, C06009, doi:10.1029/2009JC005985.

Toledo, Y., T.-W. Hsu, and A. Roland (2012), Extended time-dependent mild-slope and wave-action equations for wavebottom and wave-current interactions, *Proc. R. Soc. London A*, *468*, 184–205, doi:10.1098/rspa.2011.0377.

Tolman, H. L. (1992), Effects of numerics on the physics in a third-generation wind-wave model, *J. Phys. Oceanogr.*, *22*(10), 1095–1111, doi:10.1175/1520-0485(1992)022<1095:EONOTP>2.0.CO;2.

Uchiyama, Y., J. C. McWilliams, and A. F. Shchepetkin (2010), Wave-current interaction in an oceanic circulation model with a vortex-force formalism: Application to the surf zone, *Ocean Modell.*, *34*(1–2), 16–35, doi:10.1016/j.ocemod.2010.04.002.

Umgiesser, G., D. M. Canu, A. Cucco, and C. Solidoro (2004), A finite element model for the Venice Lagoon. Development, set up, calibration and validation, *J. Mar. Syst.*, *51*(1–4), 123–145, doi:10.1016/j.jmarsys.2004.05.009.

Warner, J. C., C. R. Sherwood, R. P. Signell, C. K. Harris, and H. G. Arango (2008), Development of a three-dimensional, regional, coupled wave, current, and sediment-transport model, *Comput. Geosci.*, *34*(10), 1284–1306, doi:10.1016/j.cageo.2008.02.012.

Wolf, J. (2009), Coastal flooding: Impacts of coupled wave-surge-tide models, *Nat. Hazards*, *49*, 241–260, doi:10.1007/s11069-008-9316-5.

Xia, H., Z. Xia, and L. Zhu (2004), Vertical variation in radiation stress and wave-induced current, *Coastal Eng.*, *51*(4), 309–321, doi:10.1016/j.coastaleng.2004.03.003.

Xie, L., K. Wu, L. Pietrafesa, and C. Zhang (2001), A numerical study of wave-current interaction through surface and bottom stresses: Wind-driven circulation in the South Atlantic Bight under uniform winds, *J. Geophys. Res.*, *106*(C8), 16,841–16,855, doi:10.1029/2000JC000292.

Yanenko, N. N. (1971), *The Method of Fractional Steps*, Springer, Berlin, doi:10.1007/978-3-642-65108-3.

Zhang, H., O. S. Madsen, S. A. Sannasiraj, and E. Soon Chan (2004), Hydrodynamic model with wave-current interaction in coastal regions, *Estuarine Coastal Shelf Sci.*, *61*(2), 317–324, doi:10.1016/j.ecss.2004.06.002.

Zhang, Y., and A. M. Baptista (2008a), SELFE: A semi-implicit Eulerian–Lagrangian finite-element model for cross-scale ocean circulation, *Ocean Modell.*, *21*(3–4), 71–96, doi:10.1016/j.ocemod.2007.11.005.

Zhang, Y., and A. Baptista (2008b), An efficient and robust tsunami model on unstructured grids. Part I: Inundation benchmarks, *Pure Appl. Geophys.*, *165*(11–12), 2229–2248, doi:10.1007/s00024-008-0424-7.

Zhang, Y., R. C. Witter, and G. R. Priest (2011), Tsunami-tide interaction in 1964 Prince William Sound tsunami, *Ocean Modell.*, *40*(3–4), 246–259, doi:10.1016/j.ocemod.2011.09.005.